In and out-of-plane constraint measures. Uniform description

A. Neimitz[1], M. Graba[1]
[1]*Kielce University of Technology, Kielce, Poland*
neimitz@tu.kielce.pl, mgraba@tu.kielce.pl

Introduction

In 1968 J.W. Hutchinson [1] published the fundamental work, which characterized the stress fields in front of a crack for the non-linear Ramberg-Osgood (R-O) material:

$$\sigma_{ij} = \sigma_0 \left(\frac{J}{\alpha \sigma_0 \varepsilon_0 I_n r} \right)^{\frac{1}{1+n}} \tilde{\sigma}_{ij}(\theta, n) \tag{1}$$

where r and θ are polar coordinates of the coordinate system located at the crack tip, σ_{ij} are the components of the stress tensor, J is the J-integral, n is R-O exponent, α is R-O constant, σ_o is a yield stress, ε_0 is a strain related to σ_o through the relation $\varepsilon_o=\sigma_o/E$. Functions $\tilde{\sigma}_{ij}(n,\theta)$, $I_n(n)$ must be found by solving the fourth order non-linear homogenous differential equation, independently for plane stress and plane strain [1,2]. Equation (1) is often called the "HRR solution".

In 1993 O'Dowd and Shih [3,4], proposed simplified solution for the stress field which provided more exact results for plane strain and low constraint elements than the HRR formula

$$\sigma_{ij} = (\sigma_{ij})_{HRR} + Q\sigma_0 \hat{\sigma}_{ij}(\theta). \tag{2}$$

To avoid the ambiguity during the calculation of the Q-stress, O'Dowd and Shih suggested, that the Q-stress may be evaluated at the distance $r=2J/\sigma_0$ from the crack tip at $\theta=0$. The Q-stress is computed from the following relationship:

$$Q = \frac{(\sigma_{\theta\theta})_{FEM} - (\sigma_{\theta\theta})_{HRR}}{\sigma_0} \text{ for } \theta=0 \text{ and } \frac{r\sigma_0}{J} = 2 \tag{3}$$

where $(\sigma_{\theta\theta})_{FEM}$ is the stress value calculated using finite element method (FEM) and $(\sigma_{\theta\theta})_{HRR}$ is a stress value evaluated form the HRR solution. The Q- parameter is a measure of the in-plane-constraint.

Guo extended the HRR analysis in a series of papers [5-7] to the three-dimensional (3D) case. In fact, he showed that the HRR singularity can be obtained for plane strain and plane stress only and in the 3D case the simplified, approximate formula in the form of Eq. (4) was proposed:

$$\sigma_{ij} = \sigma_0 \left(\frac{J^{far}}{\alpha \sigma_0 \varepsilon_0 I(T_z, n) r} \right)^{\frac{1}{1+n}} \tilde{\sigma}_{ij}(\theta, n, T_z) \tag{4}$$

where J^{far} is so called far–field J-integral, computed along the contour drawn at the distance far from the crack tip, where the plan stress dominates. In Guo's solution the thickness effect entered the final result through the functions $T_z(n,r,x_3)$, $I_n(n,T_z)$ and $\tilde{\sigma}_{ij}(n,\theta,T_z)$ where x_3 is the coordinate along the crack front. The computer program and results of computations of $I_n(n,T_z)$ and $\tilde{\sigma}_{ij}(n,\theta,T_z)$ functions were given by Galkiewicz and Graba [2]. The T_z parameter is defined as:

$$T_z = \frac{\sigma_{33}}{\sigma_{11} + \sigma_{22}} \tag{5}$$

The T_z parameter changes from 0 for plane stress to 0.5 for plane strain. It can be considered as an out-of-plane constraint [8]. The example results of numerical computations of T_z in front of the crack are presented in Figs 1 and 2.

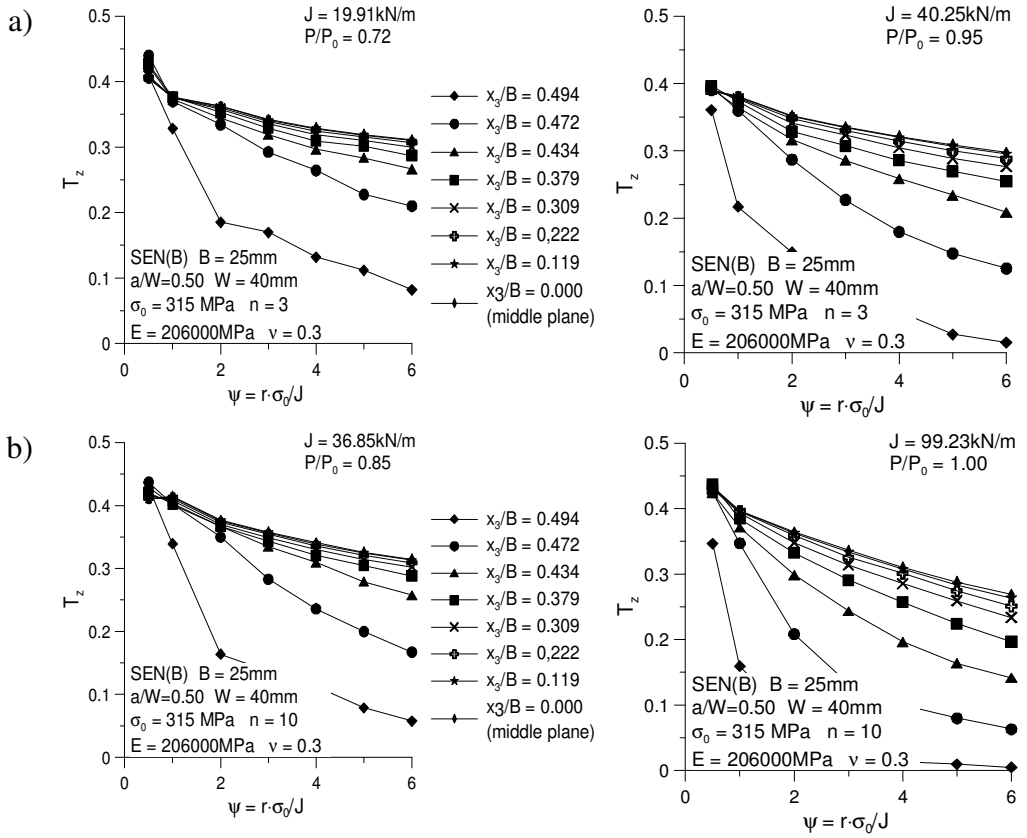

Fig. 1 Radial variation of T_z parameter for different load ratios and two work hardening exponent n. a) $n = 3$, b) $n = 10$

In- and out-of-plane constraint parameters in one formula for the stress field

We postulate that the stress fields near the crack tip can be described using two terms. Both should take into account the three-dimensional nature of the mechanical fields. The first term is the Guo term and the second one is a generalization of the *Q*-parameter. Thus, we propose the following formula:

$$\sigma_{ij} = \sigma_0 \left(\frac{J_{far}}{\alpha \sigma_0 \varepsilon_0 I_n(n,T_z) r} \right)^{\frac{1}{1+n}} \tilde{\sigma}_{ij}(\theta, n, T_z) + Q^*(n,T_z)\sigma_0 \delta_{ij} \tag{6}$$

where $Q^*(n,T_z)$ can be computed from the Eq. 8.

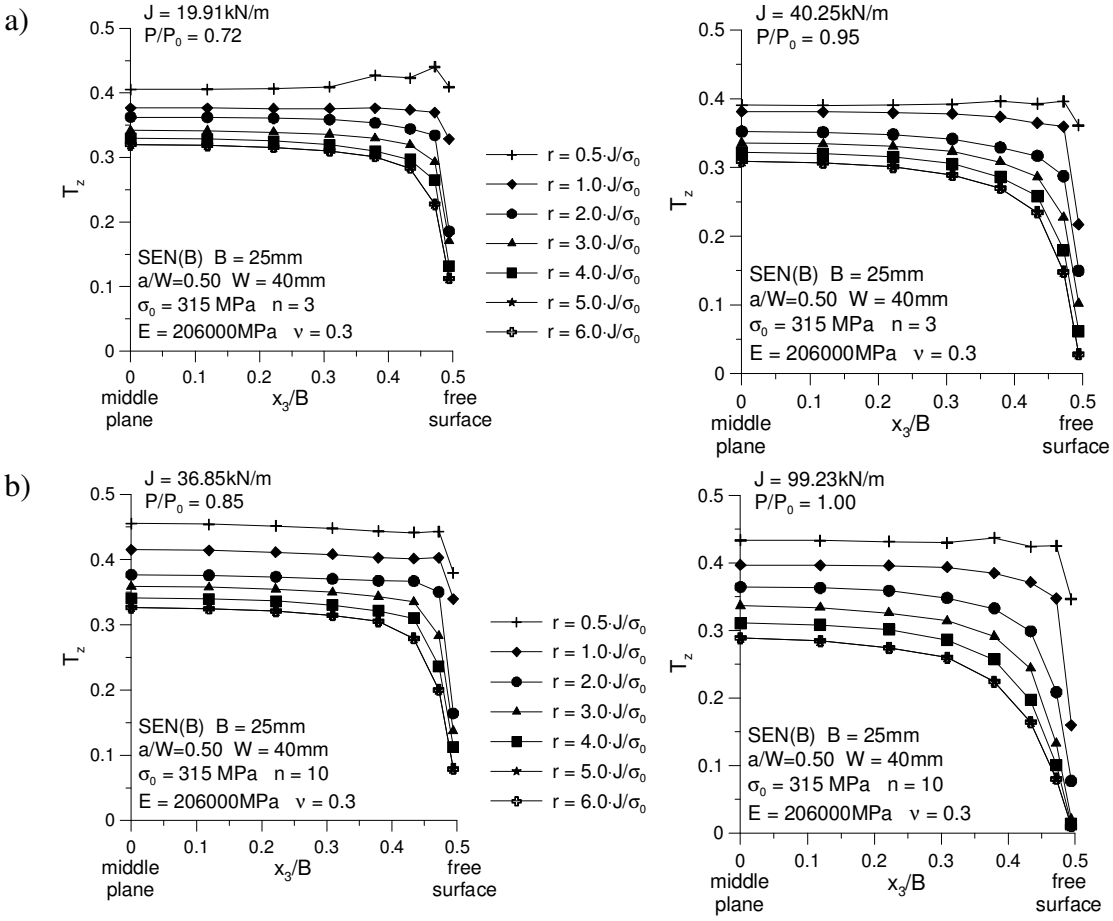

Fig. 2. Variation of T_z parameter through the specimen thickness for different load ratios and R-O exponent *n*. a) $n = 3$, b) $n = 10$

Equation 6 allows for computing σ_{ij} values at an arbitrary point in front of the 3D crack. An alternative formula, less exact but more convenient to use in practical applications is proposed in the form

$$\sigma_{ij} = \sigma_0 \left(\frac{J_{far}}{\alpha \sigma_0 \varepsilon_0 I_n(n, T_m) r} \right)^{\frac{1}{1+n}} \tilde{\sigma}_{ij}(\theta, n, T_m) + Q^*(n, T_m) \sigma_0 \delta_{ij} \tag{7}$$

where T_m function is an average through the thickness value of T_z

$$Q^*(n, Tz) = \frac{(\sigma_{\theta\theta})_{\text{FEM}} - (\sigma_{\theta\theta})_{GUO}}{\sigma_0} \quad \text{for} \quad \theta=0 \quad \text{and} \quad r = 2\frac{J}{\sigma_0} \text{ or } \frac{J}{\sigma_0} \tag{8}$$

Both the T_z and Q^* depend on a distance from the crack tip (Figs 1 and 2). Thus we compute the Q^* parameter at the distance $2J/\sigma_0$ by analogy to the O'Dowd and Shih approach as well as at the distance J/σ_0, since in the domain around this point in front of the crack, the most important failure phenomena usually take place and the maximum value of the opening stress component (the large strain option) at the large external loading ($P/P_0 \cong 1$) is located.

Details of the numerical model

The numerical analysis was performed for the single edge notched specimens in bending (SEN(B)) and for the 3D model, using a small strain option. The relative crack length was assumed a/W= 0.20 and 0.50 where a is a crack length and the width of specimens W was equal to 40mm. Computations were made using ADINA SYSTEM 8.4 [9]. Due to the symmetry, only a quarter of the specimen was modeled. The finite element mesh was filled with the 20-node 3D brick elements. The size of the finite elements in the radial direction was decreasing towards the crack tip, while in the angular direction the size of each element was kept constant. The crack tip region was modeled using 36 semicircles. The first of them was 20 times smaller then the last one. It also means, that the first finite element in front of the crack tip is 2000 times smaller then the width of the specimen. The crack tip was modeled as a half of the circle which radius was equal to r_w=5·10^{-6}m (0.000125×W). The mesh consists of eight layers of elements (through half of the thickness of the SEN(B) specimen). The layer interfaces are located at x_3/B={0 ; 0.119 ; 0.222 ; 0.309 ; 0.379 ; 0.434 ; 0.472 ; 0.494 ; 0.5}. It should be noted that the layers become thinner as the free surface is approached. The one in the middle of the specimen is twenty times thicker then the layer near the free surface. In the numerical analysis five specimen thicknesses were used: B={4, 10, 20, 25, 40}. The SEN(B) specimen was modeled using 2488 finite elements and 12142 nodes.

In the FEM simulation, the deformation theory of plasticity and the von Misses yield criterion were adopted. In the model the stress–strain curve was approximated by the relation:

$$\frac{\varepsilon}{\varepsilon_0} = \begin{cases} \sigma/\sigma_0 & \text{for } \sigma \le \sigma_0 \\ \alpha(\sigma/\sigma_0)^n & \text{for } \sigma > \sigma_0 \end{cases} \tag{9}$$

where α=1.

The tensile properties of the materials which were used in the numerical analysis are presented in Table 1. In the FEM analysis, calculations were made for twelve combinations of the yield stress and the work hardening exponent n. The J–integral was calculated using the "virtual shift method" concept. In the numerical analysis 120 SEN(B) specimens were tested.

Table 1. The mechanical properties of the materials used in numerical analysis.

σ_0 [MPa]	E [MPa]	ν	$\varepsilon_0=\sigma_0/E$
315	206000	0.3	0.00153
500			0.00243
1000			0.00485

α	n	$\tilde{\sigma}_{\theta\theta}(\theta=0)$	I_n
		for plane strain	
1	3	1.94	5.51
	5	2.22	5.02
	10	2.50	4.54
	20	2.68	4.21

Numerical results and discussion

In Fig. 3 the results obtained for several models are compared. Since we assume that the FEM results for 3D model of a specimen are the most accurate, all results are presented as a relative differences with respect to this model.

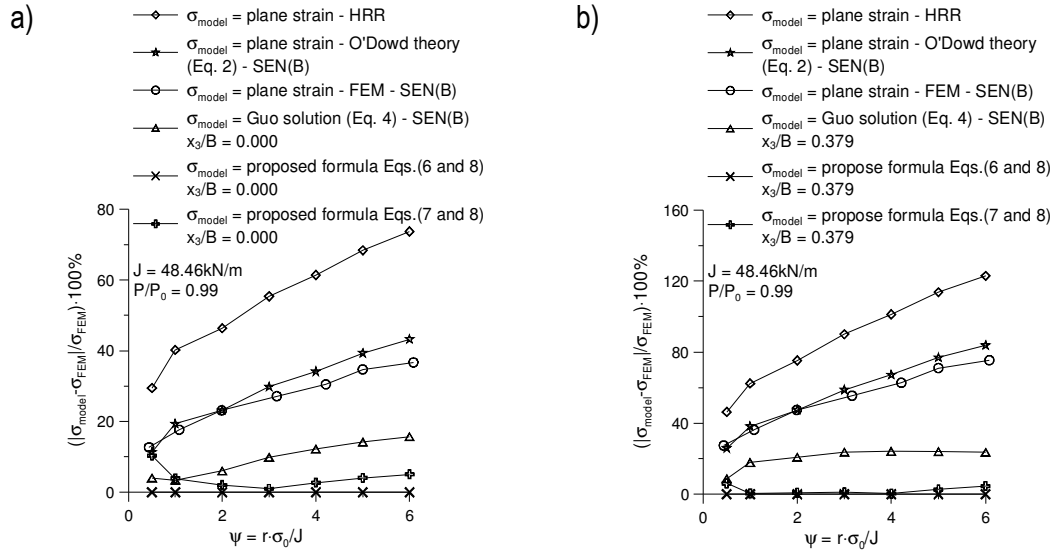

Fig.3. Comparison of results for various models of the stress field representation near the crack tip for SEN(B) specimen: a/W=0.20, B=10mm, W=40mm, σ_0=500MPa, n=10, E=206000MPa, ν=0.30, $\varepsilon_0=\sigma_0/E$=0.00243 (σ_{FEM} for x_3/B=0.000 (a) and x_3/B=0.379 (b)).

Figures 3 and 4 are representative for other results received in this research project. More results will be published soon. Notice, that the Guo's results are more exact than those received using the HRR field. Guo included into analysis

the out-of-plane constraint effect only. O'Dowd and Shih approximation as well as Yang, Chao and Sutton [11] results are also more exact than received using the HRR formula. They take into account the in-plane constraint influence only.
Eqs 6 and 7 contain both constraint measures. Results obtained with these formulas are the closest to the 3D numerical results.

Computation of the Q^* function requires numerical efforts. It depends on several variables: T_z, n, σ_0/E, distance from the crack tip, r, x_3 coordinate, the element thickness and the external loading. Also T_z function depends on many variables. However, it is possible and the research is on the way, to receive a simplified semi-analytical formulas both for the T_z (it was done for small scale yielding by Guo) and for the Q^* functions with the coefficients computed numerically. Authors of this papers are working on such a catalogue. In this paper some of the many results are presented.

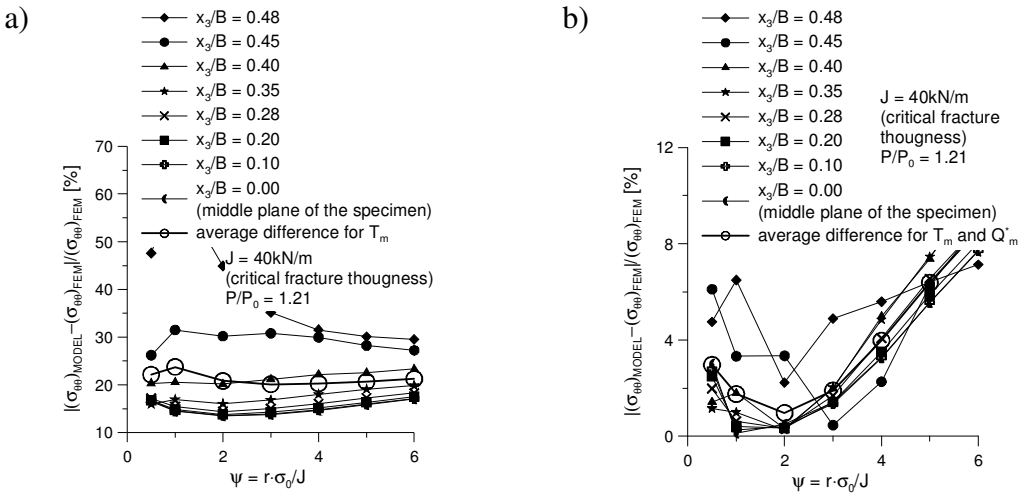

Fig.4. Comparison of results for Guo and present models with respect to the 3D FEM results a) Guo description (Eq. 4); b) proposed model by Eq. (6,8) for SEN(B) specimen: a/W=0.50, B=25mm, W=40mm, σ_0=315MPa, n=5, E=206000MPa, ν=0.30, $\varepsilon_0=\sigma_0/E$=0.00153 (P/P_0=1.21).

Aproximation of the numerical results

All the approximations were made for the two distances from the crack tip: $r=1J/\sigma_0$ and $r=2J/\sigma_0$. In the first stage the T_z function was approximated by the relation:

$$T_z(J,a,\sigma_0) = A\cdot\left(\log\frac{J}{(a\cdot\sigma_0)}\right)^3 + B\left(\log\left(\frac{J}{(a\cdot\sigma_0)}\right)\right)^2 + C\cdot\left(\log\left(\frac{J}{(a\cdot\sigma_0)}\right)\right) + D \qquad (10)$$

where the coefficients A,B,C,D were computed for each layer through the thickness and they depend on a work-hardening exponent n, a yield stress σ_0, a specimen thickness B/W and a crack length a/W. All results of the approximation

in the form of simple formulas and the look-up tables concerning the *A*,*B*,*C*,*D* coefficients will be published soon.
In this paper the example results are shown for T_m, through–the–thickness average value of T_z function. In this case the situation is simpler since the T_m=f($J/(a\cdot\sigma_0)$) function does not depend much on the R-O power exponent *n* as it is shown in Fig. 5. For the all of the 120 analyzed cases, the differences between the average curves and exact ones are not greater than 5 per cent.

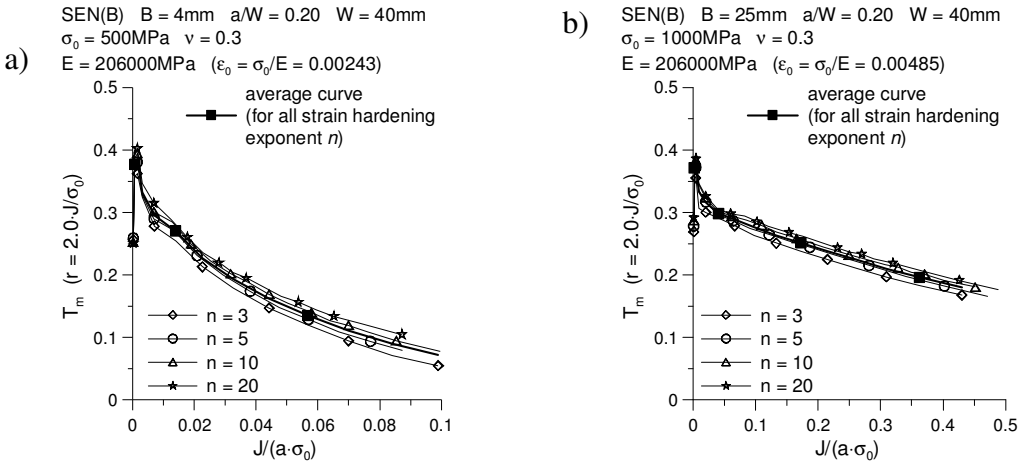

Fig.5. The T_m=f($J/(a\cdot\sigma_0)$) trajectories for two thicknesses of the SEN(B) specimens.

The T_m=f($J/(a\cdot\sigma_0)$) curves were aproximated using the following equations:

$$\ln\left(T_m\left(J,\frac{a}{W},\frac{\sigma_0}{E},\frac{B}{W}\right)\right)=A_1+\frac{B_1}{\ln\left(J/\left(a\cdot\sigma_0\right)\right)} \tag{11}$$

where A_1 and B_1 coefficients depend on a yield stress (σ_0/E), a crack length (a/W) and a specimen thickness (B/W).
In the next step, the cofficients A_1 and B_1 were expressed as the functions of B/W

$$A_1\left(\frac{a}{W},\frac{\sigma_0}{E},\frac{B}{W}\right)=C_1+D_1\cdot\left(B/W\right)+E_1\cdot\left(B/W\right)^{1.5}+F_1\cdot\left(B/W\right)^3 \tag{12}$$

$$B_1\left(\frac{a}{W},\frac{\sigma_0}{E},\frac{B}{W}\right)=C_2+D_2\cdot\left(B/W\right)+E_2\cdot\left(B/W\right)^{1.5}+F_2\cdot\left(B/W\right)^3 \tag{13}$$

where, in turn, C_1, D_1, E_1, F_1 and C_2, D_2, E_2, F_2 are functions of a yield stress and a relative crack length. Values of this cofficients are presented in the Table 2

Table 2. The values of the C_1, C_2, E1, F_1, D_1, D_2, E_2, F_2 coefficients.

***a/W*=0.20**			***r*=1.0·*J*/σ_0**
$C_1=m_1+n_1\cdot\left(\sigma_0/E\right)^2$	$D_1=m_2+n_2\cdot\left(\sigma_0/E\right)^2$	$E_1=m_3+n_3\cdot\left(\sigma_0/E\right)^2$	$F_1=m_4+n_4\cdot\left(\sigma_0/E\right)^2$

m_1=0.50316 n_1=-24392.8896 R^2=0.9999	m_2=-7.19988 n_2=135917.7796 R^2=0.9999	m_3=7.97378 n_3=-155235.707 R^2=0.9999	m_4=-1.93555 n_4=33856.76361 R^2=0.9994
$C_2 = \left[p_1 + q_1 \cdot (\sigma_0/E)^3\right]^{-1}$	$D_2 = \left[p_2 + q_2 \cdot (\sigma_0/E)^3\right]^{-1}$	$E_2 = \left[p_3 + q_3 \cdot (\sigma_0/E)^3\right]^{-1}$	$F_2 = \left[p_4 + q_4 \cdot (\sigma_0/E)^3\right]^{-1}$
p_1=0.12178 q_1=270416.0927 R^2=0.9999	p_2=-0.02192 q_2=-64078.3124 R^2=0.9998	p_3=0.01987 q_3=61602.01719 R^2=0.9993	p_4=-0.08341 q_4=-259410.142 R^2=0.9997
***a*/*W*=0.20**		***r*=2.0·*J*/σ_0**	
$C_1 = m_1 + n_1 \cdot (\sigma_0/E)$	$D_1 = m_2 + n_2 \cdot (\sigma_0/E)^{1.5}$	$E_1 = m_3 + n_3 \cdot (\sigma_0/E)^{1.5}$	$F_1 = m_4 + n_4 \cdot (\sigma_0/E)^2$
m_1=0.85345 n_1=-151.0562 R^2=0.9999	m_2=-8.21219 n_2=9656.2445 R^2=0.9999	m_3=8.95792 n_3=-11049.2828 R^2=0.9999	m_4=-2.01796 n_4=32503.7981 R^2=0.9999
$C_2 = \left[p_1 + q_1 \cdot (\sigma_0/E)\right]^{-1}$	$D_2 = p_2 + q_2 \cdot \ln(\sigma_0/E)$	$E_2 = p_3 + q_3 \cdot \ln(\sigma_0/E)$	$F_2 = p_4 + q_4 \cdot \ln(\sigma_0/E)$
p_1=0.08268 q_1=6.60593 R^2=0.9999	p_2=30.46323 q_2=13.58736 R^2=0.9997	p_3=-37.95278 q_3=-15.5037 R^2=0.9999	p_4=9.22853 q_4=3.6336 R^2=0.9999

***a*/*W*=0.50**	***r*=1.0·*J*/σ_0**	
$C_1 = m_1 + n_1/(\sigma_0/E)^{0.5} + o_1/(\sigma_0/E)$	m_1=-2.62292 n_1=0.29222	o_1=-0.0064 R^2=0.9999
$D_1 = \left[m_2 + n_2 \cdot (\sigma_0/E)^{0.5} + o_2/(\sigma_0/E)\right]^{-1}$	m_2=0.32658 n_2=-6.35980	o_2=-0.00033 R^2=0.9999
$E_1 = m_3 + n_3/(\sigma_0/E)^{0.5} + o_3/(\sigma_0/E)^2$	m_3=-9.00700 n_3=1.10311	o_3=-2.6898·10^{-5} R^2=0.9999
$F_1 = \left[m_4 + n_4 \cdot (\sigma_0/E) + o_4/(\sigma_0/E)\right]^{-1}$	m_4=0.46781 n_4=-211.7014	o_4=-0.00105 R^2=0.9999
$C_2 = p_1 + q_1 \cdot \ln(\sigma_0/E) + r_1/(\sigma_0/E)^2$	p_1=-12.09590 q_1=-4.1000	r_1=-8.0654·10^{-6} R^2=0.9999
$D_2 = \left[p_2 + q_2/(\sigma_0/E)^{0.5} + r_2/(\sigma_0/E)^2\right]$	p_2=12.63094 q_2=-4.48072	r_2=0.00011 R^2=0.9999
$E_2 = \left[p_3 + q_3 \cdot \ln(\sigma_0/E) + r_3/(\sigma_0/E)\right]^{-1}$	p_3=0.11173 q_3=0.01883	r_3=4.10433·10^{-5} R^2=0.9999
$F_2 = \left[p_4 + p_4 \cdot \ln(\sigma_0/E) + o_4/(\sigma_0/E)^{0.5}\right]^{-1}$	p_4=-0.73873 q_4=-0.16276	r_4=-0.01512 R^2=0.9999
***a*/W=0.50**	***r*=2.0·*J*/σ_0**	
$C_1 = \left[m_1 + n_1 \cdot (\sigma_0/E)^{2.5} + o_1/(\sigma_0/E)^2\right]^{-1}$	m_1=0.61061 n_1=968651.8045	o_1=1.22406·10^{-6} R^2=0.9999
$D_1 = m_2 + n_2/(\sigma_0/E) + o_2/(\sigma_0/E)^{1.5}$	m_2=2.14750 n_2=-0.07712	o_2=0.0024 R^2=0.9999
$E_1 = m_3 + n_3/(\sigma_0/E) + o_3/(\sigma_0/E)^{1.5}$	m_3=-3.54576 n_3=0.09188	o_3=-0.00286 R^2=0.9999
$F_1 = \left[m_4 + n_4 \cdot (\sigma_0/E)^{0.5} + o_4/(\sigma_0/E)\right]^{-1}$	m_4=1.57482 n_4=-27.72854	o_4=-0.00153 R^2=0.9999
$C_2 = \left[p_1 + q_1 \cdot (\ln(\sigma_0/E))/(\sigma_0/E) + r_1/(\sigma_0/E)\right]$	p_1=3.53949 q_1=0.02240	r_1=0.16095 R^2=0.9999
$D_2 = \left[p_3 + q_3 \cdot (\ln(\sigma_0/E))/(\sigma_0/E) + r_3/(\sigma_0/E)\right]$	p_2=2.93491 q_2=-0.16092	r_2=-1.1566 R^2=0.9999
$E_2 = \left[p_3 + q_3/(\sigma_0/E)^{0.5} + r_3/(\sigma_0/E)^{1.5}\right]$	p_3=-36.5277 q_3=7.978378	r_3=-0.0054 R^2=0.9999
$F_2 = \left[m_4 + n_4 \cdot \ln(\sigma_0/E) + o_4/(\sigma_0/E)^2\right]$	p_4=38.40688 q_4=9.86205	r_4=1.90215·10^{-5} R^2=0.9999

Accuracy of the approximation is high, as one can notice (R^2=0.999), Authors prepare the computer program to compute the T_m, T_z and Q^* values for arbitrary specimen sizes and material properties. The program will be available free of charge in the Internet and it will be presented during the conference. At the same time simpler, but slightly less exact formulas are beeing prepared.

The last step in the analysis is to establish the relation between Q^* (definition according to Eq.8) and T_m or T_z. We present below the selected numerical results. The numerical computations are completed but process of the approximation of these results by analytical formulas is in progress. The results of the approximations will be presented during the conference. An interesting result, which will be reflected by analytical formulas, is a relative Q_m^* independence of the external loading.

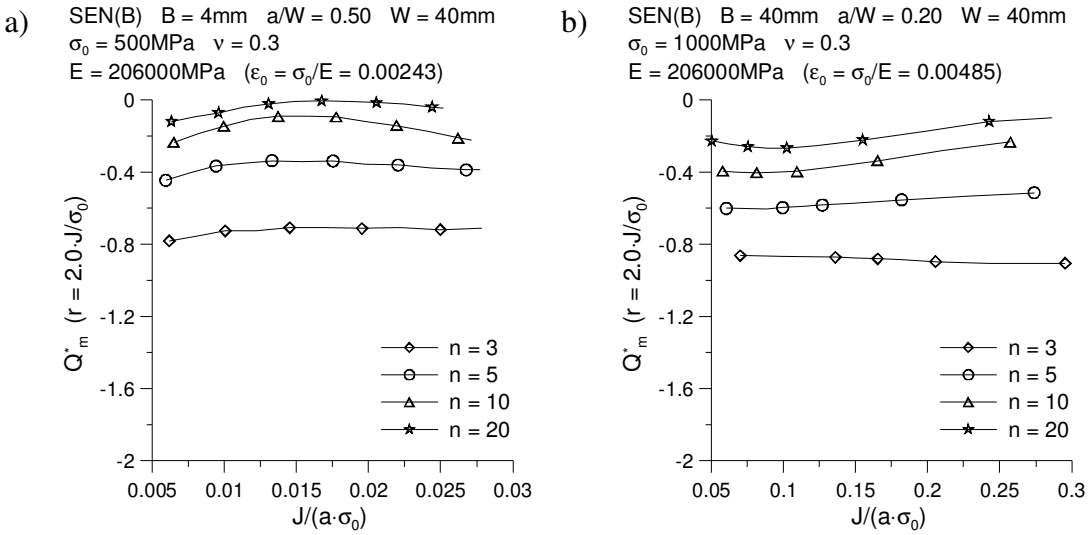

Fig.6. Q_m^*=f($J/(a\cdot\sigma_0)$) trajectories for SEN(B) specimens with thickness: a) B=4mm, b) B=40mm both measured at the distance $2J/\sigma_0$.

The strong influence of the specimen thickness on Q_m^* is observed (Fig. 7a) and moderate influence of σ_0/E (Fig. 7b)

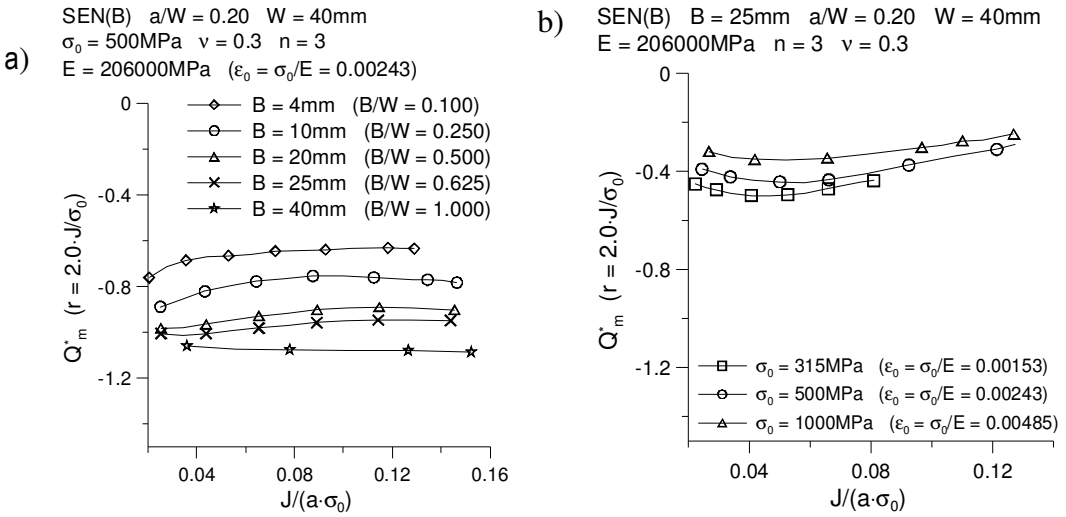

Fig.7. The Q_m^*=f($J/(a\cdot\sigma_0)$) curves for SEN(B) for various thicknesses and yield stresses.

In our research we concentrated on a relatively high external loading, which are greater than 50 per cent of the limit load. It is due to the fact that the research concerns the ferritic steels mostly.

Acknowledgements
The support of the Polish Ministry of Science and Higher Education through the grant **N504 004 31/0106** is acknowledged for the first author and **N501 264334** for the second author.

References

[1] **Hutchinson J.W.** (1968), Singular Behaviour at the End of a Tensile Crack in a Hardening Material, *Journal of the Mechanics and Physics of Solids*, 16, pp.13-31

[2] **Gałkiewicz J., Graba M.,** (2006), Algorithm for Determination of $\tilde{\sigma}_{ij}(n,\theta)$, $\tilde{\varepsilon}_{ij}(n,\theta)$, $\tilde{u}_i(n,\theta)$, $d_n(n)$ and $I_n(n)$ Functions in Hutchinson-Rice-Rosengren Solution and its 3d Generalization, *Journal of Theoretical and Applied Mechanics*, Vol. 44, No. 1, pp. 19-30

[3] **O'Dowd N.P., Shih C.F.** (1991), Family of Crack-Tip Fields Characterized by a Triaxiality Parameter – I. Structure of Fields, *J. Mech. Phys. Solids*, vol. 39, No. 8, pp. 989-1015

[4] **O'Dowd N.P., Shih C.F.** (1992), Family of Crack-Tip Fields Characterized by a Triaxiality Parameter – II. Fracture Applications, *J. Mech. Phys. Solids*, vol. 40, No. 5, pp. 939-963

[5] **Guo Wanlin** (1993), Elastoplastic three dimensional crack border field– I. Singular structure of the field, *Engineering Fracture Mechanics*, Vol. 46, No. 1, pp. 93-104

[6] **Guo Wanlin** (1993), Elastoplastic three dimensional crack border field– II. Asymptotic solution for the field, *Engineering Fracture Mechanics*, Vol. 46, No. 1, pp. 105-113

[7] **Guo Wanlin** (1995), Elasto-plastic three-dimensional crack border field– III. Fracture parameters, *Engineering Fracture Mechanics*, Vol. 51, No. 1, pp. 51-71

[8] **Neimitz A., Gałkiewicz J.** (2006), Fracture toughness of structural components: influence of constraint, *International Journal of Pressure Vessels and Piping*, Vol. 83, pp. 42-54

[9] **ASTM E 820-05**, Standard Test Method for J-integral Characterization of Fracture Toughness.

[10] **ADINA –** Theory and Modeling Guide; Report ARD 04-7; ADINA R& D, Inc.

[11] **Yang S., Chao Y.J., Sutton M.A.** (1993), Higher Order Asymptotic Crack Tip in a Power Law Hadening Material, *Engineering Fracture Mechanics*, Vol. 45, No. 1, 99. 1 – 20

[12] **Rice J.R., Rosengren G.F.** (1968), Plane Strain Deformation Near a Crack Tip in a Power-law Hardening Material, *Journal of the Mechanics and Physics of Solids*, 16, pp.1-12.